Electronic Supplementary Material (ESI) for Inorganic Chemistry Frontiers.
This journal is © the Partner Organisations 2021

Supplementary Information

Bismuth selenide nanosheets confined in thin carbon layers as anode material for advanced potassium-ion batteries

Xingxing Zhao[a,1], Chenglin Zhang[b,1], Guowei Yang[a], Yuhan Wu[b], Qun Fu[a], Huaping Zhao[b], and Yong Lei[b,]*

[a]Institute of Nanochemistry and Nanobiology, School of Environmental and Chemical Engineering, Shanghai University, Shanghai 200444, China.

[b]Fachgebiet Angewandte Nanophysik, Institut für Physik & IMN MacroNano, Technische Universität Ilmenau, 98693 Ilmenau, Germany.

*E-mail: yong.lei@tu-ilmenau.de.

[1]Xingxing Zhao and Chenglin Zhang contributed equally to this work.

Keywords: Bi_2Se_3, Anode, Potassium-ion battery, Electrochemical performance

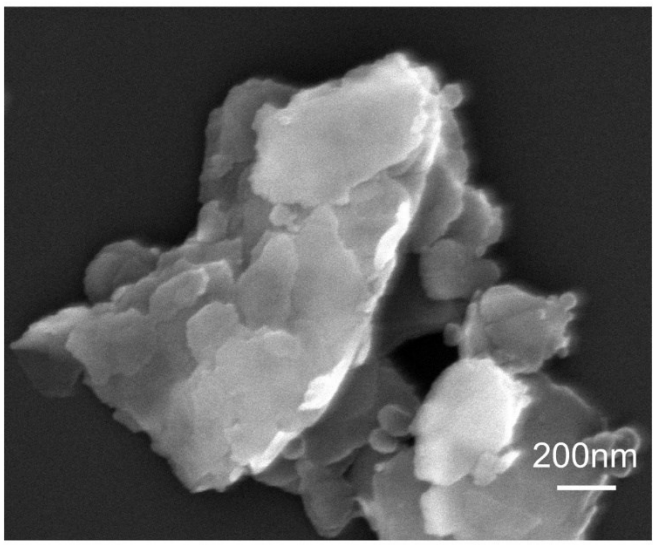

Figure S1 SEM images of Bi_2Se_3.

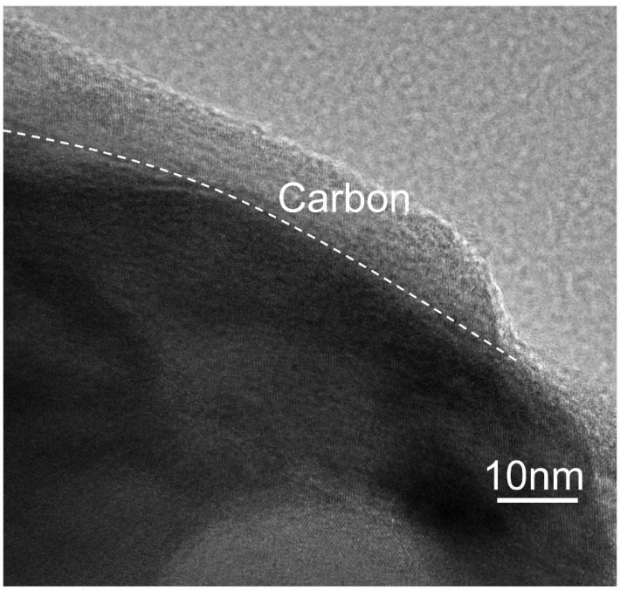

Figure S2 TEM images of Bi_2Se_3@C.

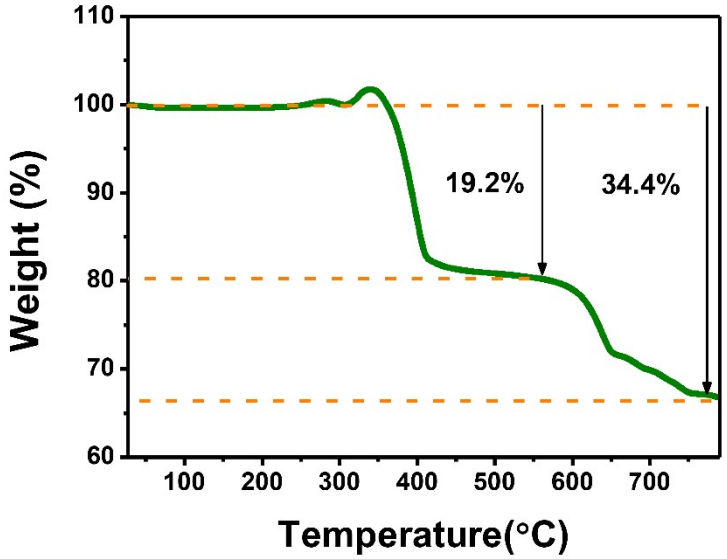

Figure S3 Thermogravimetric analysis of Bi_2Se_3@C.

In the TGA curve, the weight loss of Bi_2Se_3@C is 34.4%. The Bi_2Se_3@C first experiences a weight increase because of the oxidation reaction of Bi2Se3 to Bi_2O_3 and SeO_2. Second, the carbon is oxidated to CO_2 and the SeO_2 product is volatilized at high temperature. The final product is only Bi_2O_3. The weight loss from pure Bi_2Se_3 to Bi_2O_3 is 28.9% according to the equation (1):

$Bi_2Se_3 + C + 11/2O_2 \rightarrow CO_2 + 3SeO_2 + Bi_2O_3$

Therefore, the weight loss can be illustrated as the equation (2):

$28.9\% (1-W) + W = 34.4\%$

Where W represents the loading content of carbon, (1-W) represents the loading content of Bi_2Se_3. Thus, the content of carbon I the samples can be calculated as ~8%.[1,2]

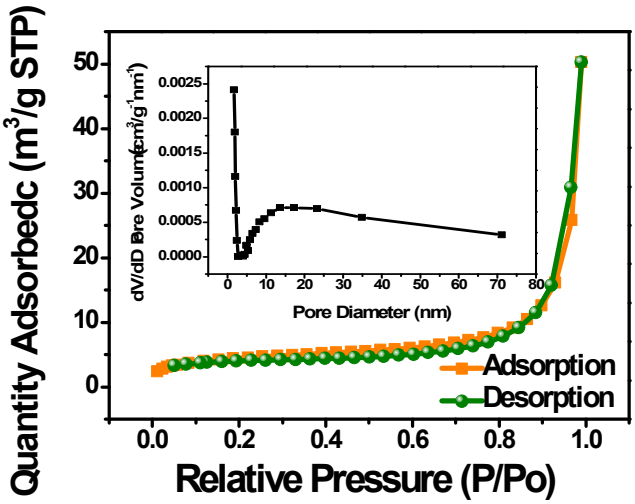

Figure S4 Nitrogen adsorption isotherm and pore size distribution (insert) of Bi_2Se_3@C.

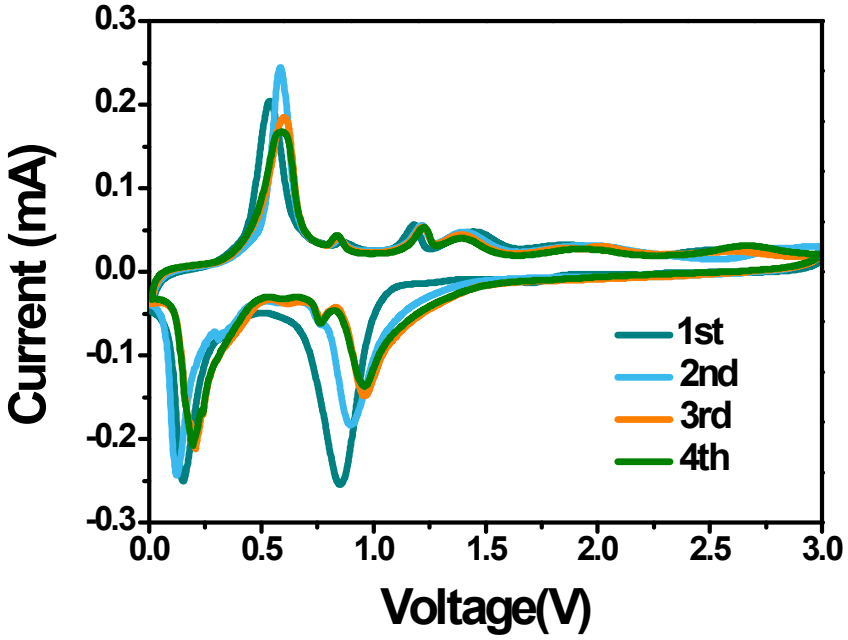

Figure S5 Initial four CV curves of Bi_2Se_3 electrode at a scan rate of 0.1 mV s^{-1} in a potential range from 0.01 to 3V.

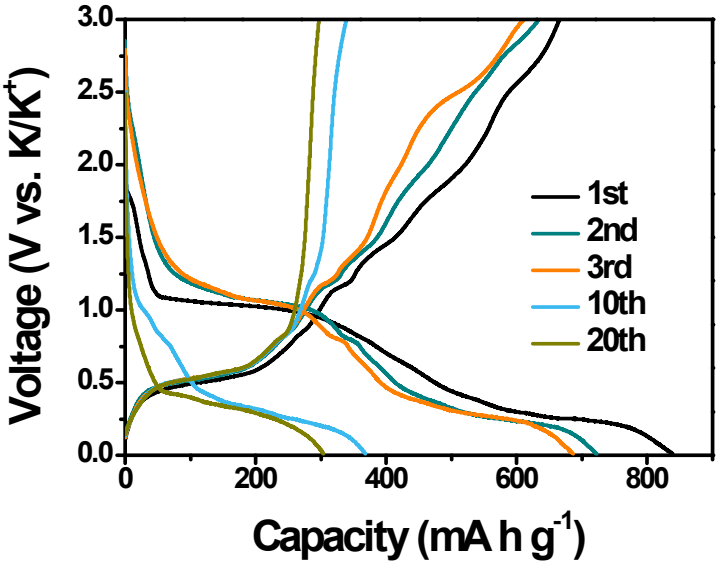

Figure S6 Discharge and charge profiles of Bi_2Se_3 within the potential of 0.01–3V at a current density of 100 mA g^{-1}.

Table S1 Comparison of some representative anodes in potassium-ion batteries.

Samples	Initial coulombic efficiency	Cyclic stability at a low current density	Rate capability		Cyclic stability at a high current density.	Ref.
			Capacity	Current densities		
Bi_2Se_3@C	**74%**	**397 mAh g^{-1} at 0.1 A g^{-1} after 100 cycles.**	**568, 446, 374, 311, 268, 210 and 526 mAh g^{-1}**	**0.05, 0.1, 0.2, 0.5, 1.0, 2.0 and 0.05 A g^{-1}**	**214 mAh g^{-1} at 1 A g^{-1} after 1000 cycles.**	**This work**
Co_3O_4@N-C	48.2%	448.7 mAh g^{-1} at 0.05 A g^{-1} after 40 cycles.	after the stage 0.1-2 C rate test, returns to 408.2 mAh g^{-1}	0.1, 0.2, 0.5, 1.0, 2.0 and 0.1 C	213 mAh g^{-1} at 0.5 A g^{-1} after 740 cycles.	3
1D/2D C_3N_4/rGO	Null	Null	after the stage 0.1-2 A g^{-1} rate test, returns to 534.1 mAh g^{-1}	0.1, 0.2, 0.5, 1.0, 2.0 and 0.1 A g^{-1}	228.6 mAh g^{-1} at 10 A g^{-1} after 1000 cycles.	4
$MoSe_2$@NCT	Null	247 mAh g^{-1} at 0.1 A g^{-1} after 100 cycles.	after the stage 0.1-2 A g^{-1} rate test, returns to 240 mAh g^{-1}	0.1, 0.2, 0.5, 1.0, 2.0 and 0.1 A g^{-1}	74 mAh g^{-1} at 1 A g^{-1} after 600 cycles.	5
NPCP@$MoSe_2$	Null	325 mAh g^{-1} at 0.1 A g^{-1} after 80 cycles.	322, 296, 283, 221, 172, 134 and 310 mAh g^{-1}	0.1, 0.2, 0.5, 1.0, 2.0, 5.0 and 0.1 A g^{-1}	128 mAh g^{-1} at 0.5 A g^{-1} after 1000 cycles.	6
Sn-MoS_2/C	88%	239 mAh g^{-1} at 0.1 A g^{-1} after 50 cycles.	375, 233, 214, 162, 123 and 310 mAh g^{-1}	0.05, 0.1, 0.2, 0.5, 0.8 and 0.05 A g^{-1}	Null	7
SnSSe/MGS	73.5%	271 mAh g^{-1} at 0.1 A g^{-1} after 500 cycles.	460, 435, 399, 330, 270, 219 and 405 mAh g^{-1}	0.1, 0.2, 0.5, 1, 2, 5 and 0.1 A g^{-1}	Null	8
V_5Se_8@C	58.6%	378 mAh g^{-1} at 0.2 A g^{-1} after 300 cycles.	328, 316, 293, 257, 201, 162 and 319 mAh g^{-1}	0.1, 0.2, 0.5, 1, 2, 4 and 0.1 A g^{-1}	145 mAh g^{-1} at 4 A g^{-1} after 800 cycles.	9
MoS_2@C	Null	241 mAh g^{-1} at 0.1 A g^{-1} after 20 cycles.	876, 306, 203, 135, 98 mAh g^{-1}	0.05, 0.1, 0.2, 0.5, 0.8 A g^{-1}	214 mAh g^{-1} at 1 A g^{-1} after 400 cycles.	10
$MoSe_2$@CNTs	69.3%	320.9 mAh g^{-1} at 0.1 A g^{-1} after 100 cycles.	354.8, 339.4, 293.0, 264.4, 245.3, 209.7, 186.1 and 401.2 mAh g^{-1}	0.1, 0.2, 0.5, 1.0, 2.0, 5.0, 10.0 and 0.1 A g^{-1}	159 mAh g^{-1} at 2 A g^{-1} after 200 cycles.	11
$MoSe_2$/N-C	79.9%	258.2 mAh g^{-1} at 0.1 A g^{-1} after 300 cycles.	300, 244, 211, 195, 178 and 300 mAh g^{-1}	0.1, 0.2, 0.5, 1.0, 2.0, 5.0 and 0.1 A g^{-1}	Null	12
CuS@GO	43.2%	290.5 mAh g^{-1} at 0.1 A g^{-1} after 100 cycles.	407.7, 322.75, 291.4, 256.2, 196.5 and 400 mAh g^{-1}	0.1, 0.2, 0.3, 0.5, 1.0 and 0.1 A g^{-1}	Null	13
MoS_2/C@NDG	59.3%	Null	343.2, 229.6, 176.6 and 300.8 mAh g^{-1}	0.5, 1.0, 2.0 and 0.3 A g^{-1}	220.7 mAh g^{-1} at 1 A g^{-1} after 150 cycles.	14

$FeMoSe_4$@NC	65%	298 mAh g^{-1} at 0.2 A g^{-1} after 100 cycles.	313, 309, 282 227 and 298 mAh g^{-1}	0.1, 0.2, 0.5, 1.0 and 0.1 A g^{-1}	178 mAh g^{-1} at 1 A g^{-1} after 150 cycles.	[15]
Sb_2Se_3@ RGO	49%	286.6 mAh g^{-1} at 0.1 A g^{-1} after 80 cycles.	557.5, 376.4, 325.4, 248.0, 173.3, 118.6 and 558 mAh g^{-1}	0.05, 0.1, 0.2, 0.5, 1.0, 2.0 and 0.05 A g^{-1}	203.4 mAh g^{-1} at 0.5 A g^{-1} after 460 cycles.	[16]
$FeSe_2$	50%	330 mAh g^{-1} at 0.1 A g^{-1} after 100 cycles.	326, 278, 234, 206, 178, 135 and 356 mAh g^{-1}	0.1, 0.2, 0.5, 1.0, 2.0, 5.0 and 0.1 A g^{-1}	128 mAh g^{-1} at 2 A g^{-1} after 500 cycles.	[17]
CoSe@NrGO	Null	218 mAh g^{-1} at 0.2 A g^{-1} after 100 cycles.	364, 357, 342, 302, and 166 mAh g^{-1}	0.2, 0.5, 1.0, 2.0 and 5.0 A g^{-1}	143 mAh g^{-1} at 2 A g^{-1} after 100 cycles.	[18]

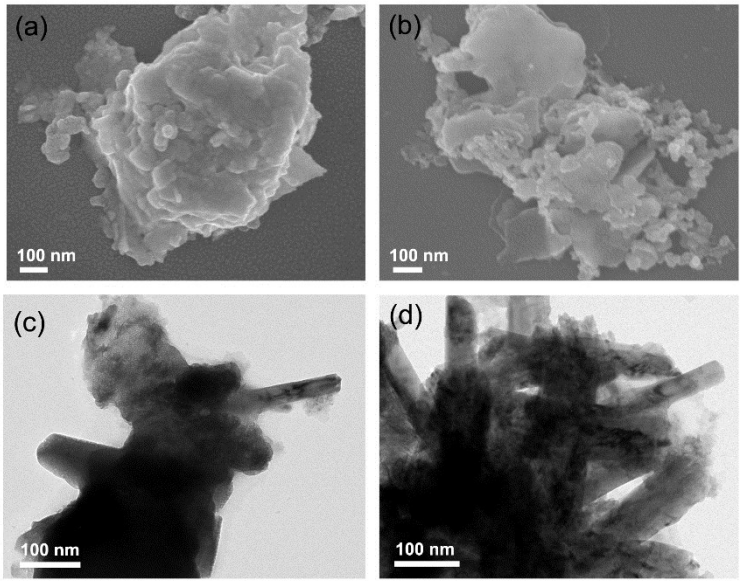

Figure S7 SEM images of (a) Bi_2Se_3 and (b) Bi_2Se_3@C after 20 cycles. The corresponding TEM images of (c) Bi_2Se_3 and (d) Bi_2Se_3@C.

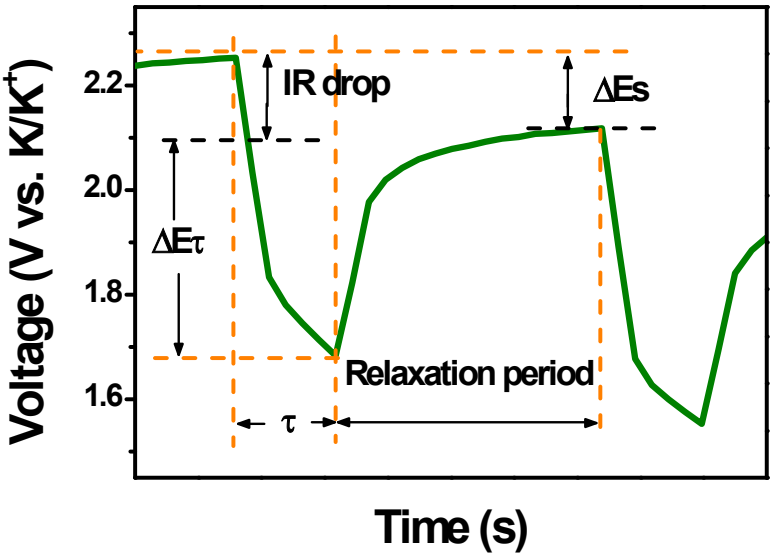

Figure S8 Schematic illustration of selected steps from the GITT profile during charging

The transfer of K^+ obeys the Fick's second law, the diffusion coefficient can be calculated by the following equation:

$$D_K = \frac{4}{\pi\tau}\left(\frac{m_B V_M}{A M_B}\right)^2 \left(\frac{\Delta E_s}{\Delta E_t}\right)^2 \left(\tau \ll \frac{L2}{D}\right)$$

where τ is the duration time of the current pulse, V_M is the molar volume ($cm^3\ mol^{-1}$), m_B is the mass of the active material, M_B is the molecular weight ($g\ mol^{-1}$), A is the total contact area of electrode with electrolyte, ΔE_τ is the variation of the cell voltage, and ΔE_s is related to the change of steady-state voltage for the corresponding step.

References

1. D. Li, J. Zhou, X. Chen and H. Song, ACS Appl. Mater. Interfaces, 2018, 10, 30379–30387.
2. L. X. Xie, Z. Yang, J. Y. Sun, H. Q. Zhou, X. W. Chi, H. L. Chen, A. X. Li, Y. Yao and S. Chen, Nanomicro Lett, 2018, 10, 50.
3. D. Adekoya, H. Chen, H. Y. Hoh, T. Gould, M. S. J. T. Balogun, C. Lai, H. Zhao and S. Zhang, *ACS Nano*, 2020, **14**, 5027–5035.

4. D. Adekoya, M. Li, M. Hankel, C. Lai, M.-S. Balogun, Y. Tong and S. Zhang, *Energy Storage Mater.*, 2020, **25**, 495–501.
5. N. N. Li, L. Sun, K. Wang, J. Zhang and X. H. Liu, *Electrochim. Acta*, 2020, **360**, 136983.
6. 4. Q. Jiang, L. Wang, Y. Wang, M. Qin, R. Wu, Z. Huang, H. J. Yang, Y. Li, T. Zhou and J. Hu, *J. Colloid Interface Sci.*, 2021, **600**, 430–439.
7. D. G. Yin, Z. Chen and M. Zhang, *J. Phys. Chem. Solids*, 2019, **126**, 72–77.
8. Z. Y. Yi, J. Y. Xu, Z. H. Xu, M. Zhang, Y. N. He, J. C. Bao and X. S. Zhou, *J. Energy Chem.*, 2021, **60**, 241–248.
9. C. Yang, F. Lv, K. Dong, F. L. Lai, K. N. Zhao, F. Sun, S. M. Dou, Q. Wang, J. Xu, P. P. Zhang, T. Arlt, X. D. Chen, Y. N. Chen, I. Manke and S. J. Guo, *Energy Storage Mater.*, 2021, **35**, 1–11.
10. Z. Chen, S. L. Chen, H. F. Zhang, M. Q. Liu, Z. J. Feng, X. B. Li, J. T. Huang and D. Guo, *Ionics*, 2020, **26**, 1779–1786.
11. Y. H. Wu, Q. C. Zhang, Y. Xu, R. Xu, L. Li, Y. L. Li, C. L. Zhang, H. P. Zhao, S. Wang, U. Kaiser and Y. Lei, *ACS Appl. Mater. Interfaces*, 2021, **13**, 18838–18848.
12. J. Ge, L. Fan, J. Wang, Q. Zhang, Z. Liu, E. Zhang, Q. Liu, X. Yu and B. Lu, *Adv. Energy Mater.*, 2018, **8**, 1801477.
13. X. X. Jia, E. J. Zhang, X. Z. Yu and B. A. Lu, *Energy Technology*, 2020, **8**, 1900987.
14. J. Zhang, P. Cui, Y. Gu, D. Wu, S. Tao, B. Qian, W. Chu and L. Song, *Adv. Mater. Interfaces*, 2019, **6**, 1901066.
15. J. Chu, Q. Yu, D. Yang, L. Xing, C. Y. Lao, M. Wang, K. Han, Z. Liu, L. Zhang, W. Du, K. Xi, Y. Bao and W. Wang, *Appl. Mater. Today*, 2018, **13**, 344–351.
16. Z. Yi, Y. Qian, J. Tian, K. Shen, N. Lin and Y. Qian, *J. Mater. Chem. A*, 2019, **7**, 12283–12291.
17. W. Zhao, Q. Tan, K. Han, D. He, P. Li, M. Qin and X. Qu, *J. Phys. Chem. C*, 2020, **124**, 12185–12194.
18. Y. Liu, K. Cui, Z. Ma and X. Wang, *Energy & Fuels*, 2020, **34**, 10196–10202.